An Enhanced Carrier-Based PWM with Reconstructed Modulation Waves for Three-Level T-type NPC Inverters in Electric Aircraft Propulsion Applications

Feng Guo*, Zhuxuan Ma, Fei Diao, Hui Cao, Yue Zhao*
Power Electronic Systems Laboratory at Arkansas (PESLA)
Department of Electrical Engineering, University of Arkansas
Fayetteville, AR, 72701, United States
Emails: fengg@uark.edu, yuezhao@uark.edu

***Abstract*—A novel carrier-based PWM (CBPWM) strategy is proposed in this paper for a three-level T-type neutral-point-clamped (3L-TNPC) inverter in electric propulsion applications. For a civil aircraft, the performance during the cruising stage, which is usually the longest in the typical mission profile with lower-rated output power, relies on high-efficiency electric propulsion. Meanwhile, its high reliability is realized on the premise of balanced neutral-point (NP) voltage. To leverage the above advantages at the same time, in this paper, by adopting the reconstructed modulation signals, not only can the NP voltage ripple be mitigated, but also the switching losses are reduced effectively. Furthermore, the active capacitor voltage balancing capability can be achieved by injecting adaptive zero-sequence voltage (ZSV) in specific intervals of pulse trains. The results of simulation and experimental test validate the effectiveness and feasibility of the presented modulation algorithm for electric aircraft propulsion applications.**

***Index Terms*—Electric aircraft propulsion drives, enhanced modulation signals, neutral-point voltage balancing, switching loss reduction, three-level topology.**

I. Introduction

Aiming at a more electrified green thrust for future airborne transportation, the state-of-the-art multilevel converters play a significant role in the electrical power conversion between the onboard electric power system (EPS) to the propulsion motor [1]. One of the interesting architectures is to combine aircraft electric starter/generator (ESG) systems investigated in [2] and [3] and turboelectric propulsion drives. Therefore, prior to cranking the generator via a coupled shaft, the aircraft turbofan engine can be activated electrically. Fig.1 displays the nominal turboelectric distributed propulsion (TeDP) system studied in this work. As can be seen, two ESG systems consisting of a permanent magnet synchronous machine (PMSM) and a bi-directional active-front-end (AFE) convert the shaft mechanical power to the electrical form feeding to an onboard dc distribution bus. It is worth noting that the bipolar structure with $\pm$ 0.5 kV is selected as it can suit onboard propulsive and non-propulsive loads simultaneously. To improve the output power quality, reduce dv/dt and lower electromagnetic interference (EMI) while using the minimum switch counts for this application, instead of other multilevel power electronics

This work was supported in part by the U.S. National Science Foundation (NSF) under CAREER Award ECCS-1751506

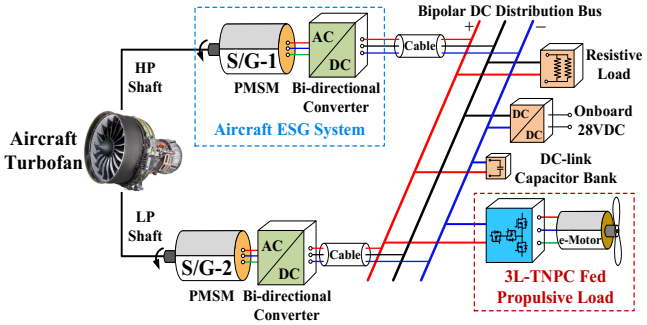

Fig. 1: The target aircraft TeDP architecture.

building blocks (PEBBs), such as cascaded H-bridge (CHB) [4], [5], active NPC (ANPC) [6], [7] and multi-port converter [8], [9] or two-level PEBB with active gate-driver [10]-[12], a T-type three-level inverter shown in Fig.2 is prototyped, in which the silicon-carbide (SiC) switching device is selected because of its high blocking voltage and low switching loss compared with silicone ones [13], [14]. A high-speed electric propulsion motor is fed by this high-power inverter, featuring a fundamental frequency of up to a kilohertz. The overall control block diagram for the studied aircraft TeDP system can be found in Fig.3. It involves motor speed control that regulates the speed of the propeller, flux-weakening control that extends inverter output capability, inner-loop current control that ensures sinusoidal ac variables, droop control that adjusts the voltage level on ESP and the PWM modulator which is the core investigated objective of this work.

Nevertheless, as a result of the split dc-link capacitors of the NPC topology, the NP potential fluctuation or deviation occurs in certain operational conditions, especially under a higher modulation index (MI) and a lower power factor (PF). This can overstress the switching devices and lead to distorted output voltage. To deal with these problems, numerous research works from the perspective of PWM strategies have been carried out in recent years. Among them, balanced NP voltage can be attained by employing the nearest-three-virtual-space-vector (NTV^2) strategy [15] and many of its variants [16]-[19]. However, this benefit is achieved at the cost of additional switching losses. Although the thermal issue is not a standing-out problem when exploiting the traditional seven-segment pulse train and can be further alleviated by the discontinuous counterpart, both ac and dc voltage offsets exist in the mid-

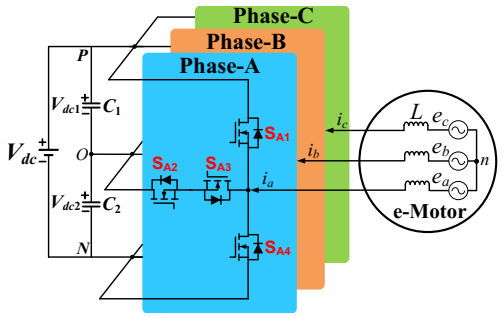

Fig. 2: Circuit diagram of 3L-TNPC.

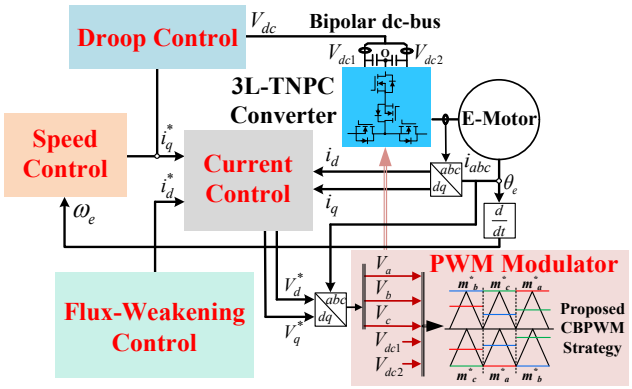

Fig. 3: Control blocks of the TeDP system.

point of dc-link, which puts the lifetime of capacitor banks at risk. In the works of [20], with constant clamping one-phase voltage for the nine-segment pulse pattern, a modified NTV^2 scheme is proposed to reduce switching losses. Nevertheless, it should be pointed out that the implementation of this PWM algorithm is complicated and the direct commutation from the positive dc-rail to the negative one happens in some scenarios. In [21], while a hybrid modulation scheme is proposed to relieve the unnecessary losses by NTV^2 in low MI region, an additional loss of 33% would still be produced in the high-speed power generating mode.

To this end, in this paper, an enhanced carrier-based PWM (CBPWM) technique is introduced for a 3L-TNPC inverter used in the aircraft's next-generation TeDP system when executing the cruise. Through reconstructing modulation waves, the proposed modulation solution can inherit exceptional NP voltage balance capability by the 3L phase voltage clamping as similar to the NTV^2 scheme but with simple implementation, while an adaptive discontinuous PWM (DPWM) method is adopted in specific intervals to reduce unnecessary switching actions. Furthermore, two types of flexible ZSVs are injected under the feedback control to correct two deviated capacitor voltages once the voltage difference exists unexpectedly.

II. The Conventional NTV^2 Strategy for 3L-TNPC Inverter

Fig.2 presents the circuit diagram of the 3L-TNPC topology, where each phase consists of four switches, i.e., S_{x1}~S_{x4}, x={A, B or C}. in which phase x denotes phase-A, B or C. Two identical capacitors, i.e., C_1 and C_2, are series-connected

TABLE I: Switching Principle of The 3L-TNPC Inverter

Switching States	Gating Signals (S_{x1},S_{x2})	Output Voltages
[P]	(1, 1)	V_{dc}/2
[O]	(0, 1)	0
[N]	(0, 0)	$-V_{dc}$/2

to form the onboard main dc-bus. Similar to the classic diode-clamped NPC converter, there are 27 switching states produced by [P], [O] and [N] by three individual phase legs. $+V_{dc}$ refers to S_{x1} and S_{x2} are ON, null voltage output mean that S_{x2} and S_{x3} are ON, and $-V_{dc}$ indicates that S_{x3} and S_{x4} are ON. Table I summarizes this switching principle.

In each sector, the conventional NTV^2 strategy applies five virtual-space-vectors (VSVs) producing average net-zero NP currents [15], as referred to V_{ZO}, V_{ZS1}, V_{ZS2}, V_{ZM}, V_{ZL1} and V_{ZL2} in Sector-I of Fig.4, in order to synthesize V_{ref}, thereby gaining NP potential balance and minimizing its ripple in every switching period. Nevertheless, in comparison with the seven-segment PWM, one of the drawbacks of this modulation method is the additional switching actions, which renders [P]→[O]→[N] in one of phase legs.

On the other hand, the computation burden of such switching patterns by VSVs is heavy if the PWM interrupt service routine is shortened, particularly for the wide bandgap (WBG)-based converter applications.

III. Proposed CBPWM Technique with Reconstructed Modulation Waves

In order to simplify the modulation process, the equivalent CBPWM is an effective alternative to generate the same switching pattern as its space-vector counterpart.

Here, taking Sector-I as an example, the dedicated modulation signals through (1) are derived prior to modifying the NTV^2, where V_a, V_b and V_c are sinusoidal voltage signals, m_a^*, m_{b1}^*, m_{b2}^* and m_c^* refer to auxiliary reference voltages.

$$\begin{cases} m_a^* = (V_a - V_b)/2 \\ m_{b1}^* = (V_b - V_c)/2 \\ m_{b2}^* = (V_b - V_a)/2 \\ m_c^* = (V_c - V_a)/2 \end{cases} \tag{1}$$

It is noticeable that the modulation wave for phase-B is then decomposed to attain 3L dc-bus voltage clamping intervals, as shown in Fig.5. In contrast, two-level clamping intervals of phase-A and C are available to reconstruct according to the optimized objectives. Herein, discontinuous pulse trains are properly configured to compensate for the extra switching actions in phase-B. For the first sector, generic ZSVs yielded in (2) are then flexibly injected into three-phase modulation signals expressed by (1).

$$\begin{cases} V_{zsv.p} = k(1 - V_{max}) + (1 - k)(-1 - V_{min}) \\ V_{zsv.n} = (1 - k)(1 - V_{max}) + k(-1 - V_{min}) \end{cases} \tag{2}$$

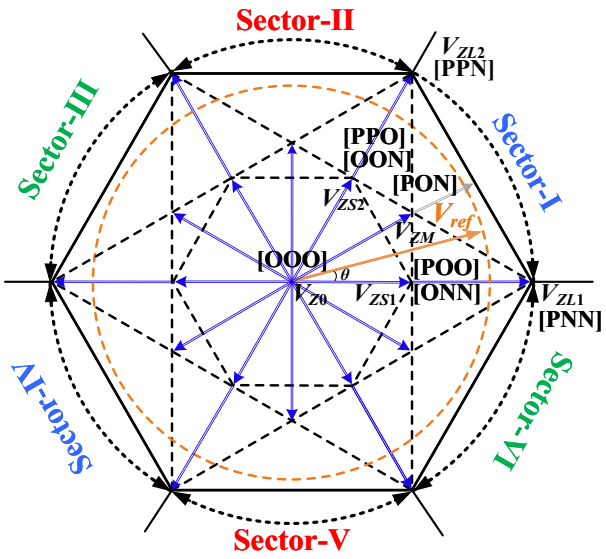

Fig. 4: Space-vector diagram of the NTV^2 strategy.

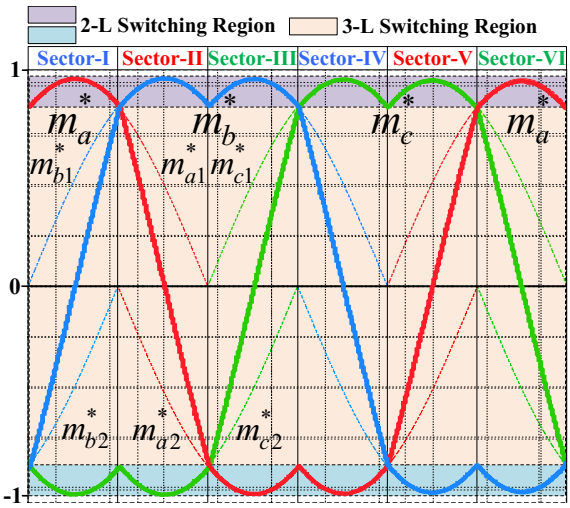

Fig. 5: Re-division of the carrier-based VSV implementation.

where V_{max} and V_{min} refer to the maximum and minimum reference voltage waves, respectively. $V_{zsv.p}$ and $V_{zsv.n}$ correspond to the case of $V_{dc1}>V_{dc2}$ and $V_{dc1}<V_{dc2}$, respectively.

It is apparent that when k equals 0.5, the conventional space-vector modulation can be equivalently attained. Another interesting finding is that when k rises up to 1, the modulation waves can seamlessly transit to the DPWM strategy and provide NP currents with different polarities. This indicates that drifted capacitor voltage can be corrected, and lower switching loss can be achieved in this region. A similar derivation can be analyzed and carried out for other sectors. The above concept forms an enhanced CBPWM that reduces the power loss of the 3L switching intervals caused by VSVs and keeps capacitor voltages balanced if an initial potential deviation exists in the midpoint of dc-link. Fig.6 shows dedicated reconstructed modulation waves and their corresponding ZSVs. As shown, the clamping region of modulated waves has a strict correlation with sector number. On the basis on NP current analysis in the works of [19], Fig.7 plots the NP currents with dual polarities associated with reference voltage rotating angles by the proposed modulation algorithm supplemented for recovering capacitor voltage divergence.

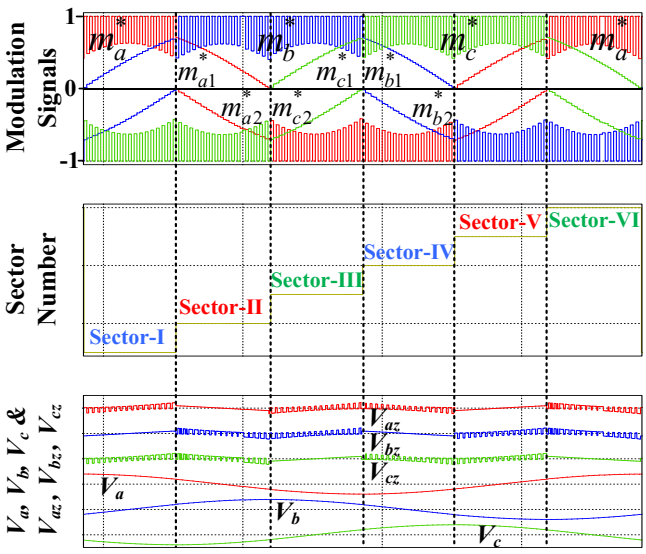

Fig. 6: The reconstructed modulation waves in different sectors.

TABLE II: Aircraft TeDP System Parameters

Parameters	Simulation	Experimentation
Rated power	1000 kVA	200 kVA
DC-bus voltage	± 540 V	± 270 V
Switching frequency	30 kHz	30 kHz
Fundamental frequency (f_0)	≤ 1 kHz	≤ 1 kHz
Capacitance (C_1=C_2)	900 μF	300 μF
Modulation index (MI)	≤ 0.95	≤ 0.95
Power factor (PF)	0.7∼1.0	0.7∼1.0

IV. Simulation and Experimental Results

The developed 1000 kVA aircraft TeDP system using a SiC-based 3L-TNPC converter is built in the MATLAB/PLECS environment, while a scaled-down setup fed RL loads is prototyped in the laboratory before a high-speed and high-power electric machine is available. The system parameters can be found in Table 1. Cree/Wolfspeed HT-3000 series 900 V power module is chosen to configure the main circuit and to analyze power losses in the following.

Fig.8 shows the state-state performance of the traditional SPWM scheme at a fundamental frequency (f_0) of 1 kHz, in which an obvious dc voltage error between two capacitor exists. Figs.9 and 10 present the modulation performance of the proposed CBPWM strategy under the steady-state at a f_0 of 400 Hz and NP voltage recovery process in the thrust-generation mode with a f_0 of 1 kHz, respectively. It can be seen that the shifted NP voltage can be kept again at a balanced state regardless of f_0, even though the two capacitor voltage imbalance initially exists. These results can demonstrate the effectiveness of the presented NP voltage balancing control ability over a variable-frequency ac output.

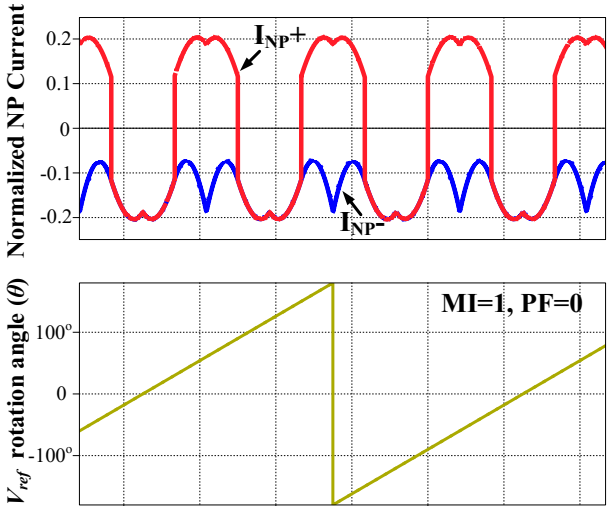

Fig. 7: NP currents by the proposed CBPWM (MI=1 and PF=0).

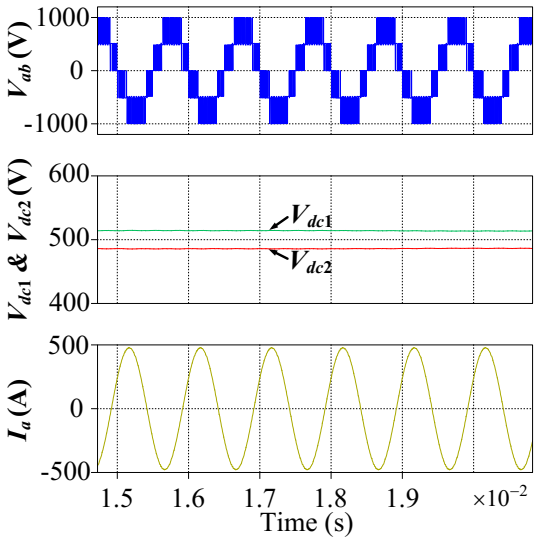

Fig. 8: The conventional SPWM method with f_0=1 kHz .

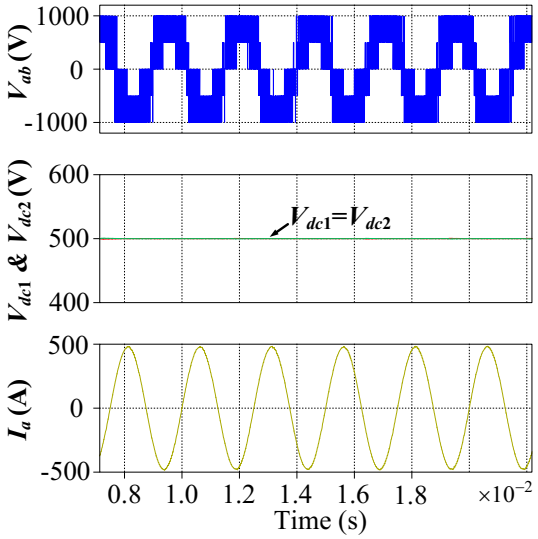

Fig. 9: The state-state by the proposed CBPWM with f_0=400 Hz.

By using the datasheet of the adopted semiconductor, the power loss analysis can be conducted through the PLECE thermal model. The specific power losses breakdown by different modulation schemes is provided in Fig.11. The results show that the switching loss by the proposed CBPWM strategy is lower than the NTV^2 strategy. By contrast, the SPWM scheme achieves the lowest switching loss because of no 3L switching intervals over a carrier period.

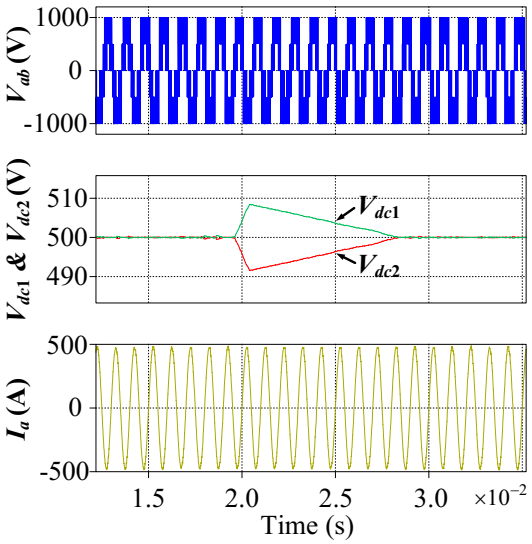

Fig. 10: The NP voltage recovery process by proposed CBPWM with f_0=1 kHz.

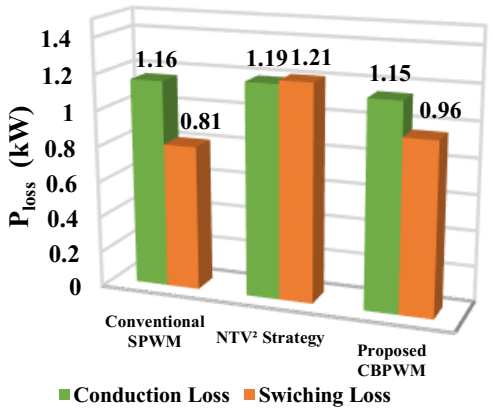

Fig. 11: Power losses breakdown by different PWM schemes.

Fig.12 displays the designed 3L-TNPC test rig that experimentally verifies the modulation performance of the proposed PWM algorithm. As capacitor voltage balance is the premise of 3L inverter normal operation, in this regard, a process of NP voltage balancing when an initial 25 V dc voltage bias exists under the conventional NTV^2 strategy is tested and presented in Fig.13. As can be seen, after switching to the proposed modulation algorithm, the NP voltage imbalance issue can be quickly restored within 10 ms, and with an output current THD of 5.47%.

V. Conclusion

This paper proposes a new CBPWM strategy with reconstructed modulation waves for the electric aircraft propulsion

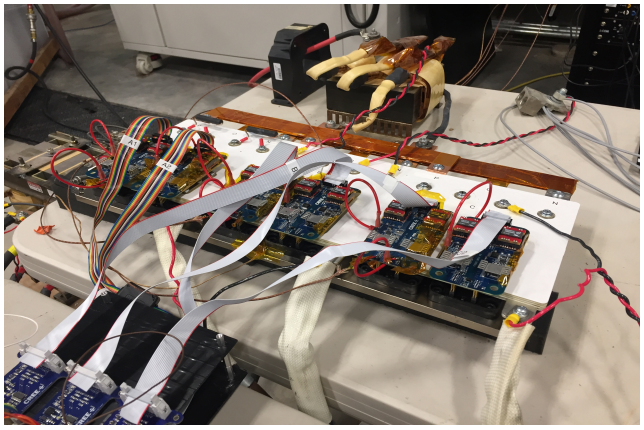

Fig. 12: The SiC-based 3L-TNPC test rig.

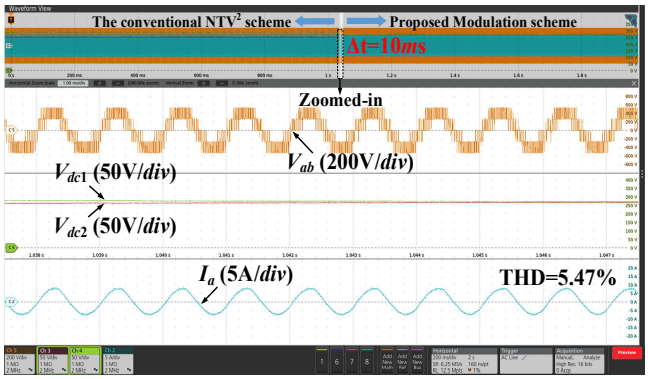

Fig. 13: NP voltage balancing process under the proposed CBPWM scheme when k=1 at MI=0.9 and PF=0.8.

system with SiC-based 3L T-type NPC power conversion stage. Aiming to reduce losses rendered by 3L switching intervals, dc-rail clamping intervals are supplemented appropriately, and also retain the capacitor voltage balancing performance. Moreover, the presented PWM algorithm is simplified in contrast with space-vector implementation. The simulation and experimental results initially validate the effectiveness and feasibility of the proposed modulation technique.

REFERENCES

[1] G. Buticchi, P. Wheeler and D. Boroyevich, "The more-electric aircraft and beyond," *Proc. IEEE*. doi: 10.1109/JPROC.2022.3152995.

[2] S. Bozhko *et al.*, "Development of aircraft electric starter–generator system based on active rectification technology," *IEEE Trans. Transp. Electrific.*., vol. 4, no. 4, pp. 985-996, Dec. 2018.

[3] F. Guo *et al.*, "An overmodulation algorithm with neutral-point voltage balancing for three-level converters in high-speed aerospace drives," *IEEE Trans. Power Electron.*, vol. 37, no. 2, pp. 2021-2032, Feb. 2022.

[4] Y. Chen, L. Du and J. He, "Online Diagnosis and Ride-Through Operation for Cascaded H-Bridge Converter Based STATCOM With a Single Open-Circuit IGBT," *IEEE Trans. Ind. Electron.*, vol. 69, no. 8, pp. 7549-7559, Aug. 2022.

[5] T. He, M. Wu, R. P. Aguilera, D. D. -C. Lu, Q. Liu and S. Vazquez, "Low computational burden model predictive control for single-phase cascaded H-bridge converters without weighting factor," *IEEE Trans. Ind. Electron.* doi: 10.1109/TIE.2022.3167133.

[6] F. Diao, Y. Li, X. Du and Y. Zhao, "An Active Hybrid Modulation Strategy for a Si/SiC Hybrid Multilevel Converter," *IEEE Open J. Power Electron.*, vol. 2, pp. 401-413, 2021.

[7] S. Belkhode, A. Shukla and S. Doolla, "Enhanced hybrid active-neutral-point-clamped converter with optimized loss distribution-based modulation scheme," *IEEE Trans. Power Electron.*, vol. 36, no. 3, pp. 3600-3612, Mar. 2021.

[8] L. Du and J. He, "A simple autonomous phase-shifting PWM approach for series-connected multi-converter harmonic mitigation," *IEEE Trans. Power Electron.*, vol. 34, no. 12, pp. 11516-11520, Dec. 2019.

[9] J. He, L. Du, S. Yuan, C. Zhang and C. Wang, "Supply voltage and grid current harmonics compensation using multi-port interfacing converter integrated into two-ac-bus grid," *IEEE Trans. Smart Grid.*, vol. 10, no. 3, pp. 3057-3070, May 2019.

[10] X. Du, J. Zeng, J. Ning, T. Kim and V. Winstead, "Modeling and Control of a Four-port DC-DC Converter for a DC Microgrid with Renewable Energy Sources," *2020 IEEE Applied Power Electronics Conference and Exposition (APEC)*, 2020, pp. 3391-3396.

[11] F. Diao, G. Zhu, Y. Wu, Y. Li, Z. Ma and Y. Zhao, "A modular and performance-tunable silicon carbide half-bridge building block with digital gate driver," *2022 IEEE Applied Power Electronics Conference and Exposition (APEC)*, Houston, TX, USA, 2022, pp. 251-258.

[12] X. Du, Y. Wei, A. Stratta, L. Du, V. S. Machireddy and A. Mantooth, "A four-level active gate driver with continuously adjustable intermediate gate voltages," *2022 IEEE Applied Power Electronics Conference and Exposition (APEC)*, Houston, TX, USA, 2022, pp. 1379-1386.

[13] H. Chen *et al.*, "Design and optimization of SiC MOSFET wire bondless power modules," *2020 IEEE 9th international power electronics and motion control conference (IPEMC2020-ECCE Asia)*, Nanjing, China, 2020, pp. 725-728.

[14] H. Chen *et al.*, "Feasibility Design of Tight Integration of Low Inductance SiC Power Module with Microchannel Cooler," *2022 IEEE Applied Power Electronics Conference and Exposition (APEC)*, 2022, pp. 962-965.

[15] S. Busquets-Monge, J. Bordonau, D. Boroyevich and S. Somavilla, "The nearest three virtual space vector PWM—a modulation for the comprehensive neutral-point balancing in the three-level NPC inverter," *IEEE Power Electron. Lett.*, vol. 2, no. 1, pp. 11-15, Mar. 2004.

[16] W. Jiang *et al.*, "A novel virtual space vector modulation with reduced common-mode voltage and eliminated neutral point voltage oscillation for neutral point clamped three-level inverter," *IEEE Trans. Ind. Electron.*, vol. 67, no. 2, pp. 884-894, Feb. 2020.

[17] F. Guo, T. Yang, A. M. Diab, S. S. Yeoh, S. Bozhko, and P. Wheeler, "An enhanced virtual space vector modulation scheme of three-level NPC converters for more-electric-aircraft applications," *IEEE Trans. Ind. Appl.*, vol. 57, no. 5, pp. 5239-5251, Sept.-Oct. 2021.

[18] S. Xia, X. Wu, J. Zheng, X. Li and K. Wang, "A virtual space vector PWM with active neutral point voltage control and common mode voltage suppression for three-level NPC converters," *IEEE Trans. Ind. Electron.*, vol. 68, no. 12, pp. 11761-11771, Dec. 2021.

[19] F. Guo, T. Yang, C. Li, S. Bozhko and P. Wheeler, "Active modulation strategy for capacitor voltage balancing of three-level neutral-point-clamped converters in high-speed drives," *IEEE Trans. Ind. Electron.*, vol. 69, no. 3, pp. 2276-2287, Mar. 2022.

[20] A. Choudhury, P. Pillay and S. S. Williamson, "DC-bus voltage balancing algorithm for three-level neutral-point-clamped (NPC) traction inverter drive with modified virtual space vector," *IEEE Trans. Ind. Appl.*, vol. 52, no. 5, pp. 3958-3967, Sept.-Oct. 2016.

[21] F. Guo *et al.*, "Hybrid active modulation strategy for three-level neutral-point-clamped converters in high-speed aerospace drives," *IEEE Trans. Ind. Electron.*, doi: 10.1109/TIE.2022.3176309